

Highly Selective High-Speed Circularly Polarized Photodiodes Based on π -Conjugated Polymers

Matthew D. Ward, Jessica Wade, Xingyuan Shi, Jenny Nelson, Alasdair J. Campbell, and Matthew J. Fuchter*

Dedicated to the memory of Professor Alasdair James Campbell

Chiral π -conjugated molecular systems that are intrinsically sensitive to the handedness of circularly polarized (CP) light potentially allow for miniaturized, low-cost CP detection devices. Such devices promise to transform several technologies, including biosensing, quantum optics, and communication of data encrypted by exploiting the spin angular momentum of light. Here a simple, bilayer organic photodiode (CP OPD) comprising an achiral π -conjugated polymer–chiral additive blend as the electron donor layer and an achiral C₆₀ electron acceptor layer is realized. These devices exhibit considerable photocurrent dissymmetry g_{ph} , with absolute values as high as 0.85 and dark currents as low as 10 pA. Impressively, they showcase a linear dynamic range of 80 dB, and rise and fall times of ≈ 7 μs , which significantly outperforms all previously reported CP selective photodetectors. Mechanistically, it is shown that the g_{ph} is sensitive to the thickness of both the chiral donor and achiral acceptor layers and that a trade-off exists between the external quantum efficiency and g_{ph} . The fast-switching speeds of these devices, coupled with their large dynamic range and highly selective response to CP light, opens up the possibility of their direct application in CP sensing and optical communications.

1. Introduction

Photonic devices that make use of circularly polarized (CP) light will revolutionize the fields of biosensing,^[1] quantum optics,^[2,3] polarization-enhanced imaging,^[4–6] microfluidics,^[7] and encrypted optical communications.^[8] Central to these applications is the ability to discriminate between left- and right-handed CP light (LH CPL and RH CPL hereafter). This is typically achieved by combining an inorganic photodetector and polarizing optical components—a configuration unsuitable for miniaturization or low-cost manufacture. As a result, recent efforts have concentrated on the design of active layers that can intrinsically detect CPL, eliminating the need for bulky, complex device architectures.

The detection of CPL is primarily achieved in two ways, 1) the manipulation of the local electromagnetic environment

with chiral plasmonic nanostructures or 2) the use of chiral molecules in active layers.^[9–12] For CP organic photodetectors (OPDs), a common figure of merit used to evaluate the selectivity of their response to the handedness of CPL is the dissymmetry or “ g ” factor, which is defined as

$$g = \frac{I_L - I_R}{\frac{1}{2}(I_L + I_R)} \quad (1)$$

Here, subscripts L and R denote LH CPL and RH CPL, respectively, and I is either the resultant absorbance or the photocurrent of the device, giving rise to the dissymmetry of absorption, g_{abs} , and dissymmetry of photocurrent, g_{ph} , respectively.^[13,14] For OPDs, other important figures of merit include external quantum efficiency (EQE), dark current, rise time (t_{rise}), and fall time (t_{fall}), which are defined in (Table S1, Supporting Information).


The recent research interest in chiral optoelectronic devices has seen the realization of several CP photodetectors based on both organic and organic–inorganic hybrid chiral systems (summarized in Table S1, Supporting Information). However, all of these systems have their own shortcomings. While devices that incorporate chiral plasmonic nanostructures can exhibit outstanding CP selectivity ($|g_{\text{ph}}| \leq 1.6$), they typically

M. D. Ward, J. Nelson, A. J. Campbell[†]
Department of Physics
Imperial College London
South Kensington Campus, Prince Consort Road, London SW7 2AZ, UK
M. D. Ward, J. Wade, X. Shi, J. Nelson, A. J. Campbell, M. J. Fuchter
Centre for Processable Electronics
Imperial College London
South Kensington Campus, London SW7 2AZ, UK
E-mail: m.fuchter@imperial.ac.uk

J. Wade
Department of Materials
Imperial College London
Exhibition Road, London SW7 2AZ, UK

X. Shi, M. J. Fuchter
Department of Chemistry and Molecular Sciences Research Hub
Imperial College London
White City Campus, 82 Wood Lane, London W12 0BZ, UK

[†]Deceased

 The ORCID identification number(s) for the author(s) of this article can be found under <https://doi.org/10.1002/adom.202101044>.

© 2021 The Authors. Advanced Optical Materials published by Wiley-VCH GmbH. This is an open access article under the terms of the Creative Commons Attribution License, which permits use, distribution and reproduction in any medium, provided the original work is properly cited.

DOI: 10.1002/adom.202101044

suffer from low EQE ($\leq 1\%$) and cannot operate in the visible spectral region.^[11,15] Their widespread application is further hindered by complex fabrication protocols, which often involve slow instrumentation (e.g., electron-beam lithography) that render the mass production of components a challenge.^[16] The device architectures that demonstrate the greatest CP selectivity (i.e., approaching $|g_{\text{ph}}| \approx 2$, perfect CP selectivity) are based on the field-effect transistor (FET) structure, but these devices suffer from low EQE ($\approx 10^{-2}\%$) and cannot be scaled up.^[10,17,18] Chiral hybrid organic–inorganic perovskite (HOIP) photodetectors have achieved impressive EQEs ($\approx 57\%$), but unfortunately, the majority of published devices demonstrate poor CP selectivity ($|g_{\text{ph}}| \approx 0.1$).^[19–21] More recently, a low-dimensional chiral HOIP has been reported that allows for high CP selectivity in the UV ($|g_{\text{ph}}| = 1.9$).^[22] Such perovskite devices face challenges relative to competitive technologies however, such as toxicity and instability. While a handful of chiral OPDs have been reported, they demonstrate modest values of $|g_{\text{ph}}|$ (≤ 0.1), and other crucial figures of merit (e.g., EQE, linear dynamic range and response times) are rarely disclosed.^[9,12,14]

Chiral π -conjugated organic systems can demonstrate large g_{abs} , as well as offering tunable optoelectronic properties and compatibility with flexible substrates. In such systems, the dissymmetric photocurrent originates from the dissymmetric absorption of the materials, which can be quantified by their circular dichroism (CD). Photoactive achiral polymer–chiral additive blends constitute a particularly attractive and versatile class, demonstrating large g_{abs} and enabling polymers that have been optimized for photodetection to be repurposed for CP discrimination without the need for novel synthesis efforts. Recently, Kim et al. combined the achiral polymer poly[3-(6-carboxyhexyl)thiophene-2,5-diyl] (P3CT) with the chiral additive 1,1'-binaphthyl to realize a CP photodiode ($|g_{\text{ph}}| = 0.1$, EQE = 18%). Unfortunately, the very slow fall times of these devices (> 250 s) makes them practically unsuitable in any frequency-domain applications.^[12] Our group and others have demonstrated high-efficiency, high-dissymmetry ($|g_{\text{El}}| \approx 1.1$) CP organic light-emitting diodes (OLEDs) based on achiral polyfluorene-based (co-)polymers blended with a chiral small-molecule (1-aza[6]helicene, hereafter aza[6]H) additive.^[23–25] We have since postulated that the origins of these chiroptical phenomena lie in the formation of a weakly ordered double-twist cylinder blue phase, where the aza[6]H serves to template the polymers into twisted fibrils with strong coupling between electric and magnetic transition dipole moments.^[26–28]

Here we report the realization of highly selective CP OPDs based on a simple, planar heterojunction architecture comprising a poly(9,9-dioctylfluorene-*alt*-bithiophene) (F8T2):aza[6]H blend electron donor layer and a C_{60} electron acceptor layer. To the best of our knowledge, these devices represent the highest photocurrent dissymmetry ever reported for a CP OPD ($|g_{\text{ph}}| = 0.72$ at zero bias), along with fast response times ($t_{\text{rise/fall}} \approx 7$ μs) that are three orders of magnitude faster than those reported for all other CP photodetecting devices. Such fast responses open up the possibility of using these devices for short-range communication using visible light.^[29] These devices represent the first CP OPDs with device performance compatible with the demands of real-world technologies and, through mechanistic device analysis, emphasize the

importance of both π -conjugated polymer structure and device architecture in the ability to differentiate LH and RH CPL.

2. Results

The use of thermal annealing to induce a giant chiroptical response in F8T2:aza[6]H blends has already been evaluated by our group, and, unless stated otherwise, we followed the optimized protocol (140 °C for 10 min in a N_2 filled glovebox, 10 wt% loading ratio of aza[6]H) for all experiments.^[26] The naming convention for LH CPL and RH CPL is illustrated in Figure S1 (Supporting Information). To ensure that the chiral phase is not impacted by the subsequent deposition of the C_{60} layer, we compared the ellipticity spectra of donor-only thin films (F8T2:aza[6]H) to those obtained for the donor–acceptor (D–A) bilayer heterojunction (F8T2:aza[6]H– C_{60}), and find no evidence of the thermally evaporated C_{60} layer disrupting the formation of the chiral phase (Figure S2, Supporting Information).

We first fabricated a series of CP OPDs of device structure indium tin oxide (ITO)/poly(3,4-ethylenedioxythiophene): polystyrene sulfonate (PEDOT:PSS)/F8T2:aza[6]H/ C_{60} /Al (Figure 1) with variable F8T2:aza[6]H thickness (t_{D} of 77–140 nm) and a fixed C_{60} layer thickness ($t_{\text{A}} = 30$ nm). Details of experimental setups for device measurements are provided in Figure S3 (Supporting Information). We previously showed that when considering thick films ($t_{\text{D}} > 150$ nm) the true g_{abs} of our annealed blend materials does not vary with thickness.^[26] The same does not hold true for the thin films ($t_{\text{D}} < 150$ nm) evaluated here, which we attribute to the strong optical interference of forward and backward traversing waves caused by multiple reflections at the substrate–film and other neighboring interfaces, typical of optically thin films.^[30] The ellipticity (Figure 1b), as well as the apparent $|g_{\text{abs}}|$ (Figure S4, Supporting Information), increases with increasing t_{D} and are equal-and-opposite for [M]- and [P]-aza[6]H blends.^[26] Irrespective of the polarization of the excitation, the EQE decreases as t_{D} increases (Figure 1c). As can be expected from the increasing g_{abs} , $|g_{\text{ph}}|$ values corresponding to the spectral region of first CD Cotton band (≈ 480 nm) increase with increasing t_{D} , from ≈ 0.15 at $t_{\text{D}} = 81$ nm to ≈ 0.41 for $t_{\text{D}} = 110$ nm (shown in Figure 1d case of an [M]-aza[6]H-doped CP OPD). We note that g_{ph} is of opposite handedness relative to the corresponding g_{abs} ; that is, donor layers that preferentially absorb RH CPL result in a higher EQE under LH CPL near the D–A interface, and vice versa. Under reverse bias (Figure 1e,f) the CP OPDs demonstrate an enhanced g_{ph} ; for example, when $t_{\text{D}} = 140$ nm, $|g_{\text{ph}}|$ increases from 0.3 (short-circuit) to 0.85 (–3 V).

Next, we evaluated the impact of the C_{60} layer ($t_{\text{A}} = 0$ –50 nm) on the device performance, using a fixed t_{D} (77 nm). At all excitation wavelengths probed, EQE initially increases with increasing t_{A} (Figure 2a), until $t_{\text{A}} \geq 40$ nm, when the EQE falls sharply (from $\approx 8\%$ to $\approx 3\%$ for $\lambda > 400$ nm). Unexpectedly, short circuit $|g_{\text{ph}}|$ for the longer-wavelength peak (corresponding to the ellipticity peak at around 540 nm) increases as t_{A} decreases (Figure 2b), reaching $|g_{\text{ph}}| \approx 0.72$ when $t_{\text{A}} = 10$ nm. This increase is coupled with a blueshift of the wavelength (λ_{ph}) at which the maximum $|g_{\text{ph}}|$ occurs ($\lambda_{\text{ph}} \approx 540$ nm at t_{A} of

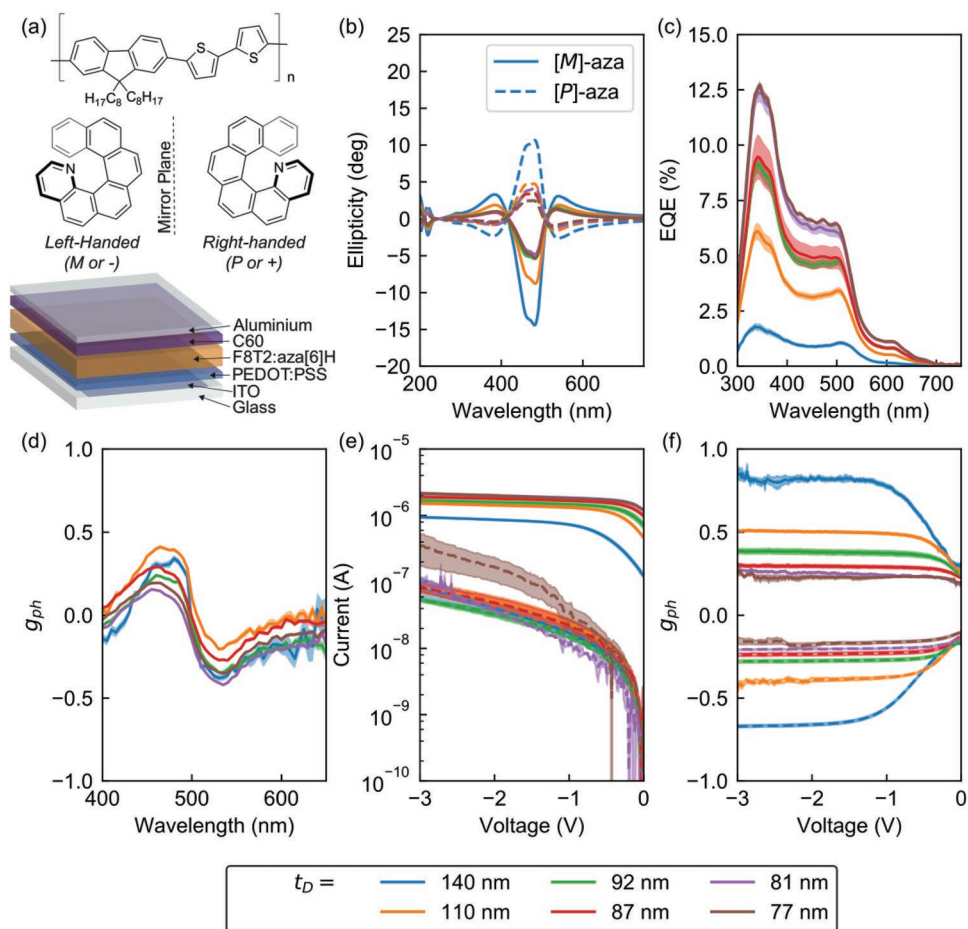


Figure 1. Influence of the blend donor layer thickness, t_D , on CP OPD performance while keeping the acceptor layer thickness at 30 nm. a) Molecular structures of F8T2 (top), [M]-aza[6]H and [P]-aza[6]H (middle), and the OPD architecture (bottom). b) Ellipticity of F8T2:[M]- (solid) and [P]-aza[6]H (dashed) blend layers. c) Unpolarized EQE and d) g_{ph} for F8T2:[M]-aza[6]H OPDs at 0 V bias. e) Current–voltage curves of F8T2:[M]-aza[6]H based OPDs under dark conditions (dashed) and unpolarized light (solid; with incident radiation 0.55 mW cm^{-2} , $\lambda_{ex} = 473 \text{ nm}$). f) g_{ph} of F8T2:[M]-aza[6]H (solid) and F8T2:[P]-aza[6]H (dashed) OPDs under reverse bias (0.21 mW cm^{-2} , $\lambda_{ex} = 473 \text{ nm}$). Shaded regions surrounding curves represent the estimated experimental uncertainty in the data.

50 nm, $\lambda_{ph} \approx 510 \text{ nm}$ at t_A of 10 nm). The relationship between g_{ph} and t_A is particularly surprising given that the presence of the achiral acceptor layer does not significantly impact the ellipticity (Figure S2, Supporting Information). We note that there is no significant enhancement of photocurrent or g_{ph} under increasing reverse bias (Figure 2c,d).

Given the trends we observed as a function of t_D and t_A , we selected two device architectures for further study: one targeting the most intense, first Cotton CD band (“1”, $\lambda = 480 \text{ nm}$; with $t_D = 87 \text{ nm}$ and $t_A = 30 \text{ nm}$) and the other targeting the longer-wavelength CD band (“2”, $\lambda = 540 \text{ nm}$; $t_D = 77 \text{ nm}$, and $t_A = 20 \text{ nm}$). These architectures maximize the difference in EQE under LH CPL and RH CPL at their target wavelengths in order to optimize both EQE and g_{ph} . In both cases, the EQE (Figure 3a) and g_{ph} (Figure 3b) are enhanced under reverse bias, reaching $|g_{ph}| > 0.1$ at an EQE of 5.2% for band 1 (solid, -1 V bias) and $|g_{ph}| > 0.4$ at an EQE of 8.4% for band 2 (dashed, -0.5 V bias). Both devices exhibit a linear response to increasing light intensity ($\lambda_{ex} = 473 \text{ nm}$) of over four orders of magnitude (Figure 3c,d), yielding linear dynamic range (LDR)

values of $\approx 80 \text{ dB}$. Under a 488-nm square-wave modulated (i.e., of on/off bistate) excitation, these devices demonstrate average rise and fall times of $\approx 7 \mu\text{s}$ (Figure 3e) and under sinusoidally varying light intensities, the bandwidths of these devices are comparable, reaching as high as 56 kHz (Figure 3f).

3. Discussion

These results not only showcase the first example of the versatile achiral polymer–chiral small-molecule additive blend systems in CP OPDs but also provide a simple platform to understand the fundamental mechanisms that underpin their device performance. The decrease in EQE with increasing t_D (Figure 1b) can be understood by considering the photogeneration and subsequent dissociation of excitons. As t_D is considerably greater than the exciton diffusion length of F8T2 ($\approx 8 \text{ nm}$), one can assume to a first approximation that statistically, most excitons generated in the donor layer more than $\approx 8 \text{ nm}$ from the D–A interface would not dissociate before annihilation, and

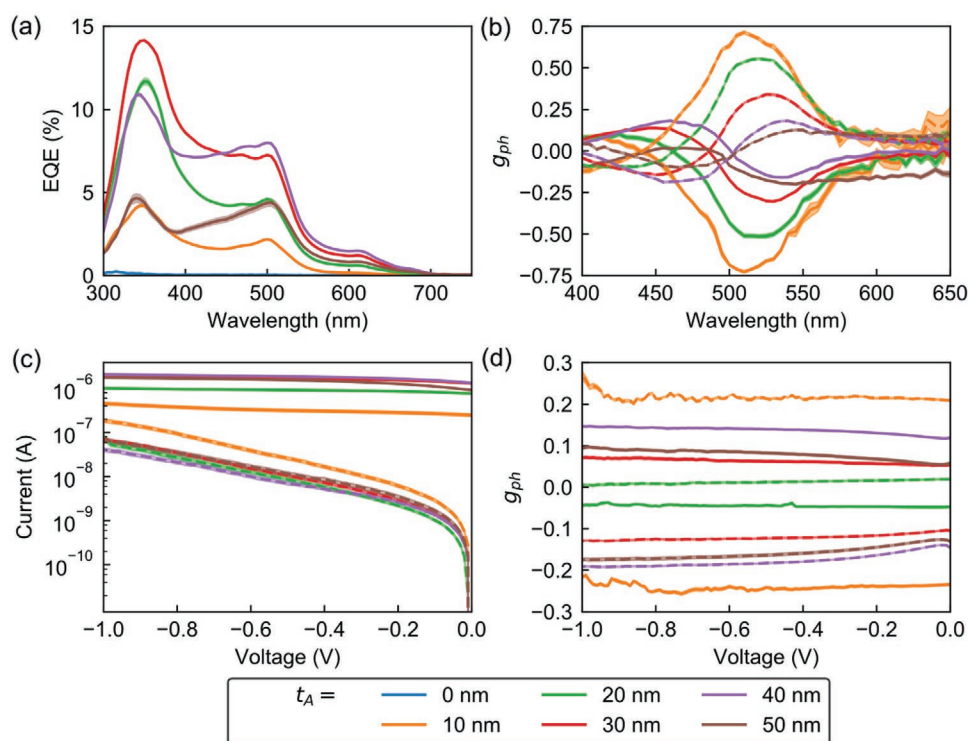


Figure 2. Influence of C_{60} acceptor layer thickness, t_A , on CP OPD performance with a fixed donor layer thickness of 77 nm. a) Unpolarized EQE and b) g_{ph} for F8T2:[M]- (solid) and [P]-aza[6]H (dashed) OPDs at zero bias. c) Current–voltage curves of F8T2:[M]-aza[6]H devices under dark conditions (dashed) and unpolarized light (solid; with incident radiation 0.57 mW cm^{-2} , $\lambda_{ex} = 473 \text{ nm}$). d) g_{ph} of F8T2:[M]-aza[6]H (solid) and F8T2:[P]-aza[6]H (dashed) OPDs under reverse bias (0.22 mW cm^{-2} , $\lambda_{ex} = 473 \text{ nm}$). Shaded regions surrounding curves represent the estimated experimental uncertainty in the data.

therefore do not contribute to the measured photocurrent.^[31] As t_D increases, the proportion of incident photons that are absorbed before they reach the D–A interface increases, and the resulting reduced light intensity at the D–A interface diminishes the EQE. On the other hand, g_{ph} increases with increasing t_D , and is always opposite in sign to g_{abs} (Figure 1b,d,f). This behavior has previously been observed using a planar heterojunction architecture by Meskers and co-workers, and can be explained by considering the mechanism illustrated in Figure 4a.^[9] For F8T2:[M]-aza[6]H devices, RH CPL is more strongly absorbed than LH CPL in the donor layer. As a result, the intensity of light that reaches the D–A interface is greater for LH CPL than it is for RH CPL, which leads to an inversion of g_{ph} relative to g_{abs} . As t_D is increased, this “filter” effect is further enhanced, which serves to increase $|g_{ph}|$. The enhancement of $|g_{ph}|$ under reverse bias, which is particularly apparent when t_D is high (Figure 1f), suggests that the efficiency of either exciton generation, exciton dissociation, or charge extraction does not increase equally with reverse bias under LH and RH CPL. Further studies are required to elucidate the precise origins of this interesting phenomenon.

While increasing t_D has a detrimental impact on device performance, the same is not true for the achiral acceptor layer (t_A) (Figure 2a,c). Consistent with an exciton diffusion length of $\approx 40 \text{ nm}$ for C_{60} , EQE and photocurrent increase until $t_A = 40 \text{ nm}$, i.e., a length until which most excitons can diffuse to the D–A interface thus contribute to the photocurrent.^[31] When the C_{60} acceptor layer thickness exceeds the exciton

diffusion length ($t_A > 40 \text{ nm}$), EQE and photocurrent decrease sharply. We attribute this to the absorption of light in the excessively thick C_{60} layer, which nonselectively reduces the light intensity that is reflected to and beyond the D–A interface from the aluminum electrode. At the same time, when the CP OPDs are excited in the low-energy band ($\approx 540 \text{ nm}$), $|g_{ph}|$ is dramatically enhanced by decreasing t_A (Figure 2b,d). We suggest that this behavior is the result of two cooperative mechanisms (Figure 4b). As described above, for F8T2:[M]-aza[6]H devices, selective absorption of RH CPL results in a greater $|g_{ph}|$ under LH CPL. The LH CPL transmitted through the achiral C_{60} layer is reflected off the back aluminum electrode, after which the handedness inverts (LH becomes RH, and vice versa). Following reflection, the CPL is the appropriate handedness to be preferentially absorbed by the chiral donor layer near the heterojunction interface. As t_A decreases, the amount of light transmitted through the acceptor layer increases, which ultimately increases g_{ph} . We attribute the lack of significant enhancement of $|g_{ph}|$ in the high-energy band (1) to the stronger absorbance of C_{60} at this wavelength (Figure S5, Supporting Information). We also observe a shift in the peak caused by band 1 from 500 nm toward 600 nm. We assign this behavior to the stronger absorbance of C_{60} at 500 nm relative to 600 nm, enabling more photons to return to the donor–acceptor interface at longer wavelengths for thicker C_{60} layers. The effect of internal reflection of CPL from the back metallic electrode has also been noted in some CP OLED works.^[32] There is an important difference between the two scenarios however: in CP OLEDs,

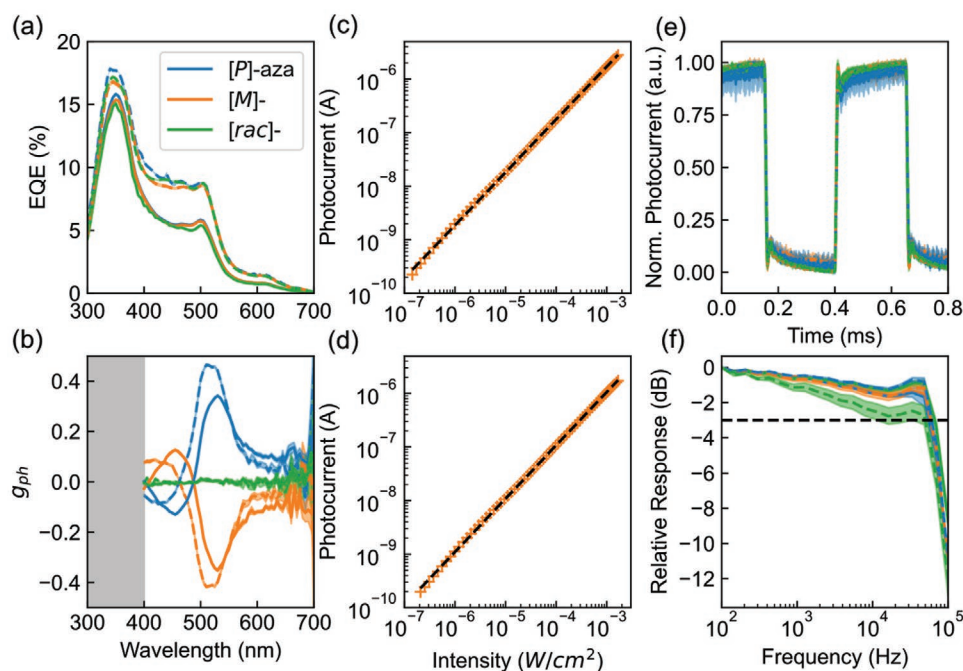


Figure 3. Device characteristics of optimized OPDs incorporating [M]-, [P]-, or [rac]-aza[6]H chiral additives. a) Reverse biased unpolarized EQE and b) reverse biased g_{ph} for OPDs fine-tuned for operation in CD band 1 (solid, -1 V bias) or CD band 2 (dashed, -0.5 V bias). Note that the quarter-wave plate used in b) does not operate at quarter-wave retardance below 400 nm (Gray). Unpolarized LDR of c) band 1-oriented OPDs and d) band 2-oriented OPDs, where dashed lines indicate the line of best fit. e) Non-CP switching response of band 1 (solid) and band 2 (dashed) OPDs under pulsing by a 2 kHz square-wave modulated laser. f) Frequency response of band 1 (solid) and band 2 (dashed) OPDs, where the horizontal black line indicates the -3 dB point where device bandwidth is determined. Incident radiation $\lambda_{ex} = 473$ nm for obtaining c) and d); and $\lambda_{ex} = 488$ nm used for e) and f). Shaded regions surrounding curves represent the estimated experimental uncertainty in the data.

reflection from the back electrode decreases the dissymmetry factor of CP emission, whereas in CP OPDs it increases the dissymmetry factor of CP detection.

The optimized devices represent an ideal balance between device performance and CP selectivity (Figure 3; and Table S1, Supporting Information). To the best of our knowledge, these

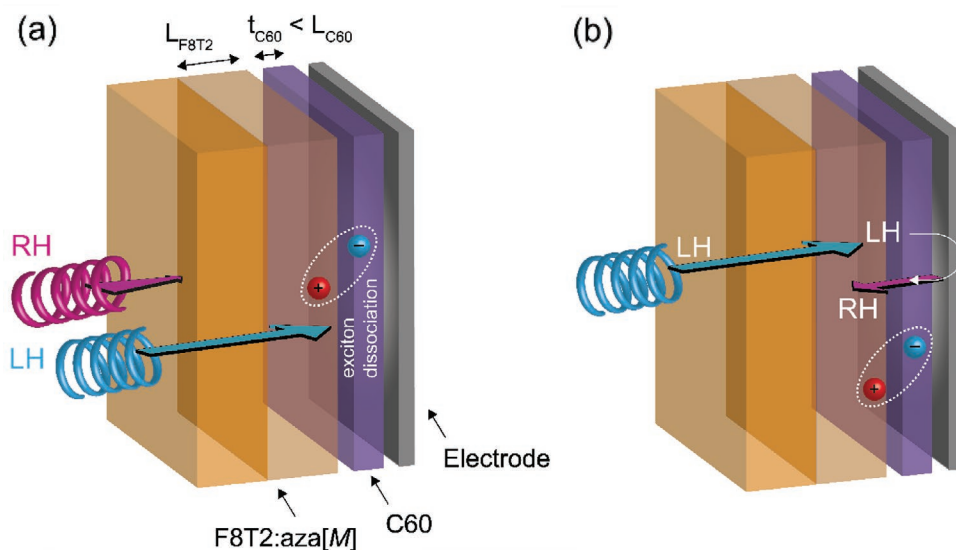


Figure 4. Proposed mechanism for the influence of a) t_D and b) t_A on CP OPD performance. For F8T2:[M]-aza[6]H devices, RH CPL is more strongly absorbed than LH CPL in the donor layer, therefore, the intensity of light that reaches the D–A interface is greater under LH CPL than RH CPL, which leads to an inversion of g_{ph} relative to g_{abs} . For thin t_A layers, the LH CPL transmitted through the achiral C_{60} layer is reflected off the back aluminum electrode, after which the handedness inverts (LH becomes RH, and vice versa). Following reflection, the CPL is of the appropriate handedness to be more preferentially absorbed by the chiral donor layer near the interface.

devices exhibit the highest LDRs (≈ 80 dB) and fastest switching times ($t_{\text{rise/fall}} \approx 7$ μs) of any CP OPDs ever reported. In particular, our switching times are three orders of magnitude faster than those reported in literature (Table S1, Supporting Information). We note that the response times of our CP OPDs correspond to a bandwidth of up to 56 kHz. Therefore, these CP OPDs could be used in conjunction with two CPL emitters for high-speed visible-light wireless communications; with two 56 kHz CPL transmission channels (LH and RH) offering a total transmission bandwidth of up to 112 kHz.^[33] Alongside increasing the speed of data transmission, the use of CPL adds an additional degree of freedom for information encryption, as any eavesdroppers using unpolarized photodetectors will only detect a meaningless superposition of LH CPL and RH CPL signals.

We present highly selective circularly polarized organic photodiodes with state-of-the-art device performance based on a chiral π -conjugated polymer donor and an achiral C_{60} acceptor in a bilayered planar heterojunction. The simplicity of this architecture allows us to investigate several interesting photophysical and chiroptical phenomena, the findings of which can inform the design of future CP-relevant materials and devices. For example, CP absorption in the donor phase and subsequent inversion upon reflection at the metallic counter electrode results in oppositely handed g_{ph} and g_{abs} . Meanwhile, g_{ph} is largest for the thinnest acceptor layers ($g_{\text{ph}} = 0.72$ when $t_{\text{A}} = 10$ nm), which we attribute to the beneficial impact of CPL inversion on the photocurrent that is greatest for the thinnest acceptor layers.

This study emphasizes that in the pursuit of high-performance, high-selectivity planar heterojunction CP OPDs, a compromise must be reached between intense g_{ph} and strong EQE. Despite this, our optimized devices demonstrate impressive figures of merit, with EQE of 5–10%, rise and fall times of ≈ 7 μs , dark currents down to 10 pA, and state-of-the-art linear dynamic ranges of ≈ 80 dB. The strong CP selectivity, coupled with very fast response times has the potential to transform many real-world applications, including CP-light encrypted, high-speed next-generation data transmission technologies, such as visible-light communications.

4. Estimation of Experimental Uncertainties

The uncertainty associated with each unpolarized EQE trace has been calculated using the standard error of the mean of measurements of 6 functionally identical OPDs. This uncertainty therefore provides an indication of device-to-device variability in a 6-device batch. Once the device-to-device variability has been quantified, 20 EQE traces are taken of one device in a 6-device batch under each circular polarization to calculate g_{ph} . This large number of repeats is required to minimize the noise in this signal (due to the small difference in EQE under LH CPL and RH CPL). The uncertainty associated with each g_{ph} spectrum is estimated as the standard error of the mean for these 20 measurements of g_{ph} for a single device.

The uncertainty associated with each unpolarized current-voltage curve and reverse bias g_{ph} plot has been calculated using

the standard error of the mean of measurements of 6 functionally identical OPDs.

The LDR plots for the band 1 and band 2 devices are traces from two representative OPDs from each 6 device batch of the band 1 and band 2 devices tested. As such, we estimate and uncertainty of 100 fA for these individual measurements, attributed to the resolution of our source-measure unit.

The uncertainty associated with both rise and fall, and bandwidth measurements represents the standard error of the mean for 6 functionally identical OPDs.

5. Experimental Section

Prepatterned 12.0×12.0 mm substrates with 145 ± 10 nm ITO on Eagle XG glass (Thin Film Devices, Inc.) were used to prepare CP OPDs with active areas of 1.5×3.0 mm². The substrates were cleaned by ultrasonication, first in acetone (15 min) followed by isopropyl alcohol (15 min) and finally a 2% concentration solution of Hellmanex III (15 min). Substrates were then subjected to 3 min of UV-Ozone treatment at a power of 80 W using an Emitech K1050X plasma asher. PEDOT:PSS was spin coated onto cleaned substrates at 3000 rpm for 30 s and then annealed at 140 °C for 15 min. Solutions of *rac*-, [*M*]-, and [*P*]-aza[6]H:F8T2 were prepared by dissolving aza[6]H and F8T2 separately in toluene at a concentration of 20 mg mL⁻¹ before combining the two with a 10 wt% loading ratio of aza[6]H. These solutions were gently heated at 70 °C for 15 min to ensure complete dissolution. The aza[6]H:F8T2 solutions were then spin-coated onto the PEDOT:PSS layer at 2000–12000 rpm for 60 s to obtain the desired film thicknesses, followed by annealing at 140 °C for 10 min to induce the strong chiroptical response in F8T2. The C_{60} donor layer and aluminum back contact were thermally evaporated onto the aza[6]H:F8T2 layer using an MBRAUN thermal evaporator and the thickness of these layers were monitored in situ using an Inficon SQM-160. The thicknesses of all device layers were verified using a Bruker DektakXT surface profilometer.

The EQE of the OPDs was measured using a Bentham PVE300 Photovoltaic Device Characterisation system. The circularly polarized EQE and g_{ph} spectra of devices was acquired using a wire-grid polariser (Thorlabs, WP25M-VIS) and a quarter-wave Fresnel rhomb retarder (Thorlabs, FR600QM).

The current-voltage and linear dynamic range characteristics of the OPDs were measured using an Agilent B2902A Precision SMU (100 fA resolution). For illuminated measurements, mounted LEDs (Thorlabs, 470 nm, M470L3; and Thorlabs, 530 nm, M530L4) were used which were collimated with an aspheric lens (Thorlabs, ACL2520U-A) and filtered with a bandpass filter (Thorlabs, 470 nm, FB470-10; or Thorlabs, 514.5 nm, FL514.5-1). For measurements of g_{ph} under reverse bias, the collimated and filtered and output of the mounted LED was circularly polarized using a wire-grid polarizer (Thorlabs, WP25M-VIS) and a zero-order quarter-wave plate (Thorlabs, 473 nm, WPQ05M-473; or Thorlabs, 514 nm, WPQ05M-514). The intensity of light incident on the OPDs was measured using a full-spectrum Si p-i-n photodiode (Hamamatsu, S1223-01).

The response time and bandwidth of the OPDs were measured using an Omicron-Laserage LightHUB-6 (488 nm) and a Stanford Instruments SR570 Low-Noise Current Preamplifier (200 kHz bandwidth, 1 $\mu\text{A V}^{-1}$ sensitivity, high bandwidth setting). The output of the current preamplifier was recorded using a Tektronix digital phosphor oscilloscope (DPO 5104B). For response time measurements, a 2-kHz square wave with 50% duty cycle was used to measure rise and fall times. For both bandwidth and response time measurements, a 2- μW beam with a diameter of 1 mm was modulated using sine waves and square waves, respectively, supplied by an Agilent 33210A 10 MHz Function/Arbitrary Waveform Generator.

Thin-film ellipticity spectra were acquired using a Chirscan from Applied Photophysics. UV-Vis spectra were measured using a Shimadzu

UV–VIS spectrophotometer (UV-2550). Calculated values of g_{abs} (Figure S4, Supporting Information) have been corrected for reflection losses using the method devised by Schulz et al.^[34]

Supporting Information

Supporting Information is available from the Wiley Online Library or from the author.

Acknowledgements

The authors thank the Engineering and Physical Science Research Council for funding through Grant Nos. EP/L016702/1, EP/R00188X/1, and EP/S515085/1. The authors would also like to thank the Worshipful Company of Scientific Instrument Makers for additional funding through the WCSIM Postgraduate Scholarship. Prof. Jenny Nelson acknowledges support from the European Research Council (ERC) under the European Union's Horizon 2020 research and innovation program (Grant No. 742708, CAPaCITY). The authors would also like to acknowledge the contributions of Dr. Jochen Brandt in the purification of F8T2 for the preliminary studies of this device architecture and Tianyi Zhang and Dr. Nicola Gasparini for providing support with device switching response and bandwidth measurements. The authors are grateful to Doug Marshall and Applied Photophysics for their support in calculating the true ellipticity in samples showing strong dissymmetry.

Conflict of Interest

A. Campbell and M. Fuchter are inventors on a patent concerning chiral blend materials (WO2014016611).

Author Contributions

M.D.W. fabricated and characterized OPDs. M.D.W. and J.W. performed thin-film analysis of constituent device layers. M.D.W. and X.S. tested switching speed and frequency response of OPDs. J.N., A.J.C., and M.J.F. supervised the project.

Data Availability Statement

The data that support the findings of this study are available from the corresponding author upon reasonable request.

Keywords

chiral materials, chiroptical response, circularly polarized light, organic photodiodes, photodetectors

Received: May 25, 2021

Revised: September 10, 2021

Published online: November 2, 2021

[1] V. Dremine, D. Anin, O. Sieryi, M. Borovkova, J. Näpänkangas, I. Meglinski, A. Bykov, *Proc. SPIE* **2020**, 11363, 3.

[2] C. Wagenknecht, C.-M. Li, A. Reingruber, X.-H. Bao, A. Goebel, Y.-A. Chen, Q. Zhang, K. Chen, J.-W. Pan, *Nat. Photonics* **2010**, 4, 549.

- [3] J. F. Sherson, H. Krauter, R. K. Olsson, B. Julsgaard, K. Hammerer, I. Cirac, E. S. Polzik, *Nature* **2006**, 443, 557.
- [4] S. S. Lin, K. M. Yemelyanov, E. N. Pugh, N. Engheta, *Conf. Proc. – IEEE Int. Conf. Networking, Sensing and Control*, Vol. 1, IEEE, Piscataway, NJ **2004**, pp. 216–221.
- [5] S. Peña-Gutiérrez, M. Ballesta, S. Royo, *Proc. SPIE* **2019**, 11059, 288.
- [6] J. S. Tyo, M. P. Rowe, E. N. Pugh, N. Engheta, *Appl. Opt.* **1996**, 35, 1855.
- [7] J. Leach, H. Mushfique, R. Di Leonardo, M. Padgett, J. Cooper, *Lab Chip* **2006**, 6, 735.
- [8] P. R. Sura, M. Sekhar, *IETE J. Research* **2021**, 0, 1
- [9] J. Gilot, R. Abbel, G. Lakhwani, E. W. Meijer, A. P. H. J. Schenning, S. C. J. Meskers, *Adv. Mater.* **2010**, 22, E131.
- [10] Y. Yang, R. C. Da Costa, M. J. Fuchter, A. J. Campbell, *Nat. Photonics* **2013**, 7, 634.
- [11] W. Li, Z. J. Coppens, L. V. Besteiro, W. Wang, A. O. Govorov, J. Valentine, *Nat. Commun.* **2015**, 6, 8379.
- [12] N. Y. Kim, J. Kyhm, H. Han, S. J. Kim, J. Ahn, D. K. Hwang, H. W. Jang, B.-K. Ju, J. A. Lim, *Adv. Funct. Mater.* **2019**, 29, 1808668.
- [13] N. Berova, L. D. Bari, G. Pescitelli, *Chem. Soc. Rev.* **2007**, 36, 914.
- [14] M. Schulz, F. Balzer, D. Scheunemann, O. Arteaga, A. Lützen, S. C. J. Meskers, M. Schiek, *Adv. Funct. Mater.* **2019**, 29, 1900684.
- [15] J. Peng, B. P. Cumming, M. Gu, *Opt. Lett.* **2019**, 44, 2998.
- [16] T. R. Groves, in *Nanolithography*, (Ed: M. Feldman), Woodhead Publishing, Cambridge **2014**, pp. 80–115.
- [17] J. Cheng, F. Ge, C. Zhang, Y. Kuai, P. Hou, Y. Xiang, D. Zhang, L. Qiu, Q. Zhang, G. Zou, *J. Mater. Chem. C* **2020**, 8, 9271.
- [18] W. Shi, F. Salerno, M. D. Ward, A. Santana-Bonilla, J. Wade, X. Hou, T. Liu, T. J. S. Dennis, A. J. Campbell, K. E. Jelfs, M. J. Fuchter, *Adv. Mater.* **2021**, 33, 2004115.
- [19] C. Chen, L. Gao, W. Gao, C. Ge, X. Du, Z. Li, Y. Yang, G. Niu, J. Tang, *Nat. Commun.* **2019**, 10, 1927.
- [20] L. Wang, Y. Xue, M. Cui, Y. Huang, H. Xu, C. Qin, J. Yang, H. Dai, M. Yuan, *Angew. Chem., Int. Ed.* **2020**, 59, 6442.
- [21] D. Li, X. Liu, W. Wu, Yu Peng, S. Zhao, L. Li, M. Hong, J. Luo, *Angew. Chem., Int. Ed.* **2021**, 60, 8415.
- [22] A. Ishii, T. Miyasaka, *Sci. Adv.* **2020**, 6, 3274.
- [23] D.-M. Lee, J.-W. Song, Y.-J. Lee, C.-J. Yu, J.-H. Kim, *Adv. Mater.* **2017**, 29, 1700907.
- [24] Y. Yang, R. C. Da Costa, D.-M. Smilgies, A. J. Campbell, M. J. Fuchter, *Adv. Mater.* **2013**, 25, 2624.
- [25] L. Wan, J. Wade, F. Salerno, O. Arteaga, B. Laidlaw, X. Wang, T. Penfold, M. J. Fuchter, A. J. Campbell, *ACS Nano* **2019**, 13, 8099.
- [26] J. Wade, J. N. Hilfiker, J. R. Brandt, L. Liirò-Peluso, Li Wan, X. Shi, F. Salerno, S. T. J. Ryan, S. Schöche, O. Arteaga, T. Jávorf, G. Siligardi, C. Wang, D. B. Amabilino, P. H. Beton, A. J. Campbell, M. J. Fuchter, *Nat. Commun.* **2020**, 11, 6137.
- [27] L. Wan, X. Shi, J. Wade, A. J. Campbell, M. J. Fuchter, *Adv. Opt. Mater.* **2021**, 9, 2100066.
- [28] B. Laidlaw, J. Eng, J. Wade, X. Shi, F. Salerno, M. J. Fuchter, T. J. Penfold, *Chem. Commun.* **2021**, 57, 9914.
- [29] H. Haas, L. Yin, Y. Wang, C. Chen, *J. Lightwave Technol.* **2016**, 34, 1533.
- [30] A. Armin, M. Hamsch, I. K. Kim, P. L. Burn, P. Meredith, E. B. Namdas, *Laser Photonics Rev.* **2014**, 8, 924.
- [31] O. V. Mikhnenko, P. W. M. Blom, T.-Q. Nguyen, *Energy Environ. Sci.* **2015**, 8, 1867.
- [32] F. Zinna, U. Giovanella, L. D. Bari, *Adv. Mater.* **2015**, 27, 1791.
- [33] A. L. Kaniolotsky, N. Laurand, M. D. Dawson, G. A. Turnbull, I. D. W. Samuel, P. J. Skabara, *Acc. Chem. Res.* **2019**, 52, 1665.
- [34] M. Schulz, J. Zabolocki, O. S. Abdullaeva, S. Brück, F. Balzer, A. Lützen, O. Arteaga, M. Schiek, *Nat. Commun.* **2018**, 9, 2413.